Chapter 11

Electronic Ferroelectricity in II-VI Semiconductor ZnO

Akira Onodera and Masaki Takesada

Additional information is available at the end of the chapter

http://dx.doi.org/10.5772/52304

1. Introduction

II-VI semiconductor Zinc oxide (ZnO) is a well-known electronic material [1-3]. Because of large piezoelectric constant and electromechanical-coupling constant, ZnO has been applied to ultrasonic transducer, SAW filter, gas sensor *etc* [3-5]. In addition, ZnO has been used widely as pigment and UV cut cosmetics extensively, so it is a safe material for our living environment, compared with heavy metals used in semiconducting process and materials science. Recently, ZnO has been studied as a material for the solar cell, transparent conductors formed on liquid crystal displays, and the blue laser [6]. Then, *p*-type ZnO was found by Joseph *et al* [7].

Ferroelectricity is recognized to appear mainly by the delicate balance between a long-range dipole-dipole interaction and a short-range interaction. When electrons should be well localized in dielectrics, the electronic distribution in the unit cell is determined by atomic positions of constituent ions. Slight distortion of electronic distribution due to structural changes in dielectrics gives a rise of dipole moments. From this point of view, the ferroelectric phase transition should be understood as a structural phase transition from the paraelectric phase with high symmetry to the ferroelectric phase with low symmetry. The atomic displacements are generally 0.01~0.1 Å, which are small compared with Bohr radius (0.53 Å). Therefore ferroelectrics are considered as a group of materials which are sensitive to structural changes. In this sense, the ferroelectric phase transition is classified into one of the structural phase transitions.

The basic Hamiltonian is generally given as

H= H(phonon) + H(electron) + H(electron-phonon),

where H(phonon) and H(electron) are due to motions of ion cores and valence electrons, and H(electron-phonon) presents interactions between ions and valence electrons. In dielec-

tric materials, the contribution of electron systems is usually omitted since the band gap is generally wide. However, it should be necessary to consider the electron-phonon interaction in the case of ferroelectric semiconductors, since the correlation energy of dipole-dipole interaction (about 0.2 eV) is comparable with band-gap energy in some narrow-gap and wide-gap semiconductors. For this type of compounds, the electronic contribution due to bond charges and conduction electrons should play a key role and must be taken into account for understanding the nature of ferroelectricity. For long time, the importance of electronic contribution has been pointed out in the field of ferroelectrics, since the simple superposition of electronic polarizability does not hold in many ferroelectric substances. Recently, the novel ferroelectricity was discovered in narrow-gap and wide-gap semiconductors such as $Pb_{1-x}Ge_xTe$ [8], $Cd_{1-x}Zn_xTe$ [9] and $Zn_{1-x}Li_xO$ [10].The appearance of ferroelectricity is primarily due to electronic origin in $Zn_{1-x}Li_xO$. Although the ferroelectric phase transition accompanies with structural distortions in usual ferroelectrics, only small structural changes of the order of 10^{-3} Å are observed in $Zn_{1-x}Li_xO$. The change in *d-p* hybridization caused by Li-substitution is responsible for the novel ferroelectricity and dielectric properties. In this chapter, we summarized recent works mainly onZnO.

2. Zinc oxide

The crystal Structure of ZnO is wurtzite-type ($P6_3mc$) as shown in Fig. 1, which belongs to hexagonal system. It does not have the center of symmetry, and is polar along the *c*-axis. Although it has been pointed out that the structure of pure ZnO has the possibility to exhibit ferroelectricity, the polarization switching does not observed until its melting point (1975°C) because of large activation energy accompanied by dipole switching process. The lattice constants are a = 3.249858 Å, c= 5.206619 Å at room temperature (298 K) [11]. Zn and O ions are bonded tetrahedrally and form ZnO_4 groups. This tetrahedron is not perfect: the apical bond length of Zn-O is 1.992 Å (parallel to the *c*-axis) and the basal one is 1.973 Å. Bond length along the *c*-axis is longer than other three bonds by 0.96%: the ZnO_4tetrahedra distort along the *c*-axis, which result in dipole moment. According to recent first-principles studies, it was reported that the hybridization between the Zn 3*d*-electron and the O 2*p*-electron plays an important role for dielectric properties of ZnO [12, 13].The energy gap E_g is 3.44 eV [14]. Although stoichiometric ZnO is an insulator (intrinsic semiconductor), it exhibits *n*-type conductivity because of excess Zn atoms. The resistivity is about 300 Ωcm, which, however, changes drastically by doping various impurities. By doping of trivalent ions, such as Al^{3+}, In^{3+}, Ga^{3+}, it reduces to the order of 10^{-4}Ωcm and shows the conductivity near that of metals [15].

Although *p*-type conductivity is expected by doping of monovalent Li^+ ions, ZnO becomes an insulator and the resistivity increases to as much as 10^{10}Ωcm [16-18]. It is remarkable that the change in resistivity reaches over the order of 10^{14}, which covers from metal-like to insulating region. It suggests that the physical nature in this material changes drastically by a little amount of dopant.

http://dx.doi.org/10.5772/52304

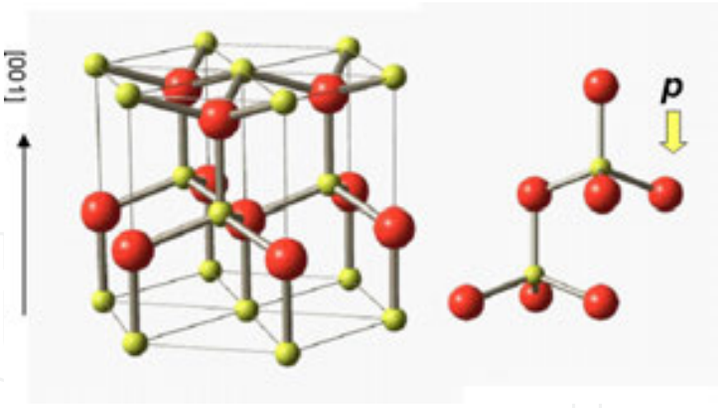

Figure 1. Crystal structure of ZnO (Wurtzite structure).

3. Electronic structure

Electronic structure of ZnO has been studied by LMTO (linear muffin-tin orbital) method [19] and by LAPW (linearized augmented-plane-wave) method using LDA (local density approximation). Band structure and the density of states is shown in Figs. 2 and 3 [20]. Around -17 eV, there are two bands originating from the O 2*s*-states. The narrow bands between -6 and -4 eV consist mainly of the Zn 3*d*-orbitals, and moderately dispersive bands from -4 to 0 eV consist mainly of the O 2*p*-orbitals. Figure 4 shows significant *d*-*p* hybridization. The 3*d* derived bands split into two groups, leading to double-peak structure in DOS (density of states). The lower peak is characterized by a strong *d*-*p* hybridization. The sharp upper peak between -4.8 and -4.2 eV has strong Zn 3*d* character and the hybridization with the O 2*p*-state is very small. Band gap is 0.77 eV. Discrepancy with the experimental value is larger than that of LMTO. It is due to the LDA gap error [21].

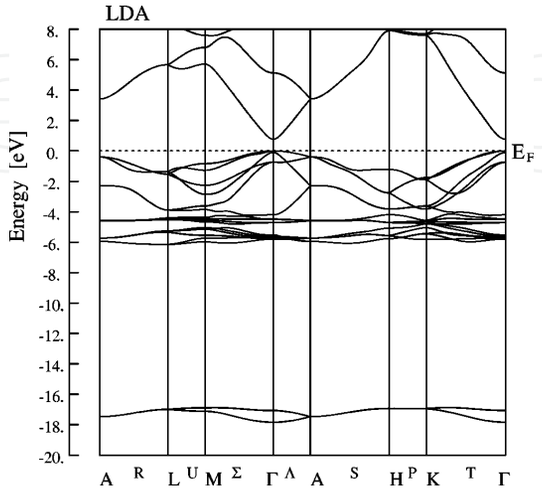

Figure 2. Band structure of ZnO using LAPW.

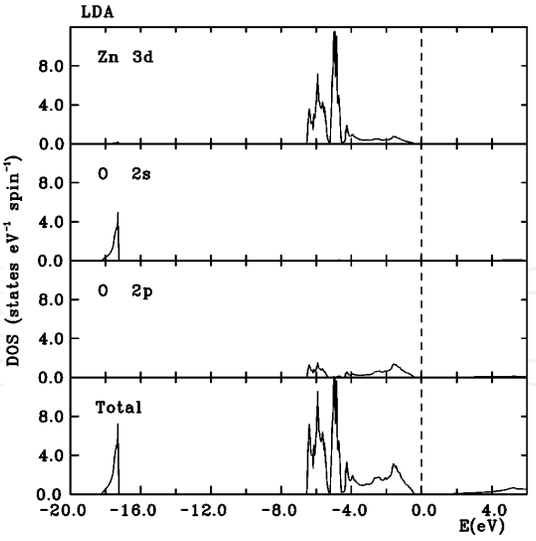

Figure 3. Density of states of ZnO using LAPW.

4. Ferroelectricity in binary semiconductors

Recently, the novel ferroelectricity was found in Li-doped ZnO [10, 22, 23], although pure ZnO has not shown any evidence of ferroelectricity. Generally representative ferroelectrics have complicate crystal structures such as Rochelle salt ($KNaC_4H_4O_6$ $4H_2O$), TGS (tri-glycine sulfate, $(NH_3CH_2COOH)_3H_2SO_4$) and $BaTiO_3$. Since ZnO is a simple binary compound, it is very convenient to study the microscopic mechanism and its electronic contribution for the appearance of ferroelectricity. Besides ZnO, IV-VI narrow-gap semiconductor $Pb_{1-x}Ge_xTe$ and II-VI wide-gap semiconductor $Cd_{1-x}Zn_xTe$, are known as materials of binary crystals accompanying ferroelectricity.

4.1. IV-VI Narrow-gap semiconductor

Among IV-VI semiconductor, $Pb_{1-x}Ge_xTe$ has been investigated extensively about its ferroelectricity [8]. $Pb_{1-x}Ge_xTe$ has a NaCl (rock-salt) type structure at room temperature. Although any ferroelectric activities have not been observed in pure PbTe and GeTe crystals, the ferroelectric phase transition is induced only in solid solution $Pb_{1-x}Ge_xTe$. In the low temperature phase of $Pb_{1-x}Ge_xTe$, the crystal becomes rhombohedral and exhibits ferroelectric activity. In the case of x = 0.003, it shows a large dielectric anomaly of the order of 10^3 at T = 100 K as shown in Fig. 5 and the softening of TO mode was observed.

The energy gap of $Pb_{1-x}Ge_xTe$ is no more than 0.3 eV, which is 3000 K in temperature. This value is comparable to the energy of the Lorentz field of dielectrics, $(4\pi/3)P$. Therefore, conduction electrons can couple strongly with phonons in this solid solution. The electron-phonon interaction decreases the frequency of TO phonon mode which results in the ferroelectric phase transition. In $Pb_{1-x}Ge_xTe$, doped Ge ions displace from the center position

http://dx.doi.org/10.5772/52304

of Pb ion by 0.8 Å and behave as *off-center ions* because of the ionic size-mismatch between Pb ion (the ionic radius: 1.2 Å) and Ge ion (the ionic radius: 0.73 Å) [24]. The direction of displacement is the eight equivalent [111] directions, which is spatially vacant and polar in the rock-salt structure. Above T_c, the ions shift toward any one of these directions at random, but its displacement would be ordered along the trigonal axis below T_c. The ordering of the *off-center ion* triggers the softening of TO phonon mode and induces rhombohedral distortion in the way such as $\cdots Pb^{2+}\text{-}Te^{2-}\cdots Pb^{2+}\text{-}Te^{2-}\cdots Pb^{2+}\text{-}Te^{2-}\cdots$or $\cdots Te^{2-}\text{-}Pb^{2+}\cdots Te^{2-}\text{-}\ Pb^{2+}\cdots Te^{2-}\text{-}Pb^{2+}\cdots$. This structural ordering generates spontaneous polarization. However, in $Pb_{1-x}Ge_xTe$, the *D-E* hysteresis loop has not been observed, while it is a direct evidence of the ferroelectricity. Whereas traditional dielectric measurements are performed on a parallel-plate capacitor, it is difficult to measure dielectric constant of such lossy $Pb_{1-x}Ge_xTe$ because of current leaks. Therefore dielectric constant is determined by the *C-V* measurement or the optical reflectiveity, which are commonly used in semiconductors. The large dielectric anomaly and soft mode of $Pb_{1-x}Ge_xTe$ suggest the ferroelectric activity.

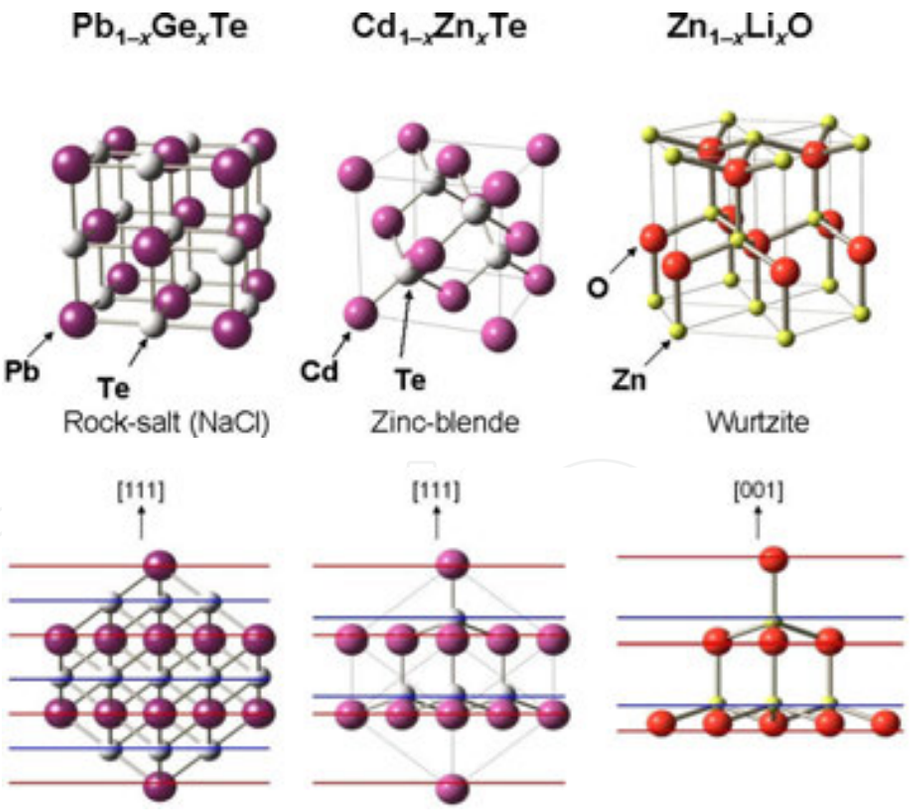

Figure 4. Crystal structures of $Pb_{1-x}Ge_xTe$, $Cd_{1-x}Zn_xTe$ and $Zn_{1-x}Li_xO$. The lower figures are plots along the polar [111] directions for $Pb_{1-x}Ge_xTe$ and $Cd_{1-x}Zn_xT$, and polar [0 0 1] direction for $Zn_{1-x}Li_xO$.

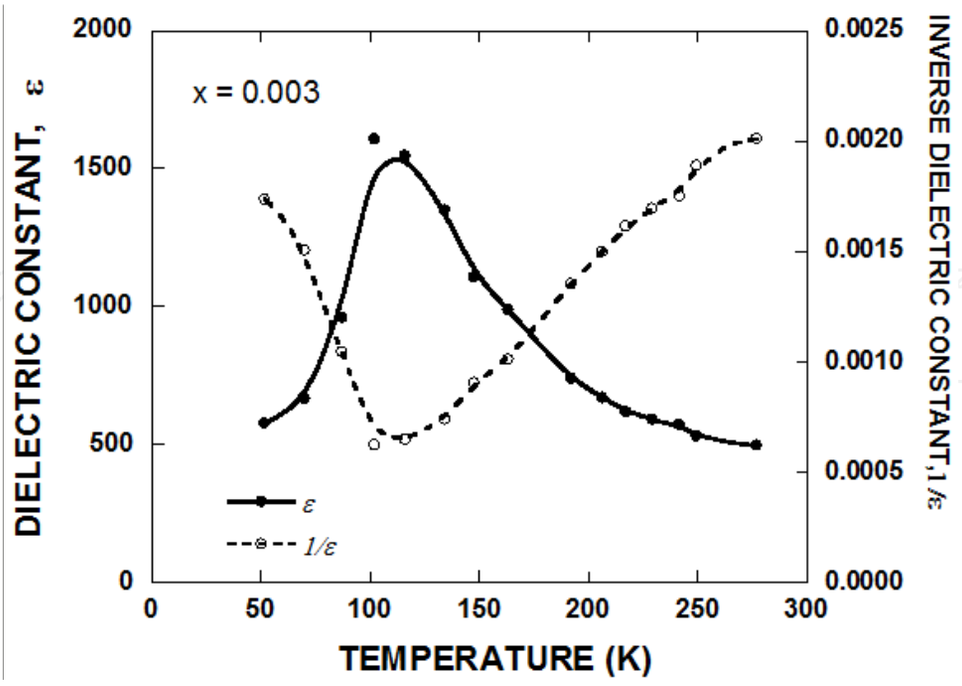

Figure 5. Temperature dependence of dielectric constant in $Pb_{1-x}Ge_xTe$ (x=0.003).

4.2. II-VI Wide-gap semiconductor $Cd_{1-x}Zn_xTe$

Among many wide-gap semiconductors, the ferroelectricity of $Cd_{1-x}Zn_xTe$ was discovered by R. Weil *et al* in 1988 [9, 25]. The E_g of $Cd_{1-x}Zn_xTe$ is 1.53 eV. It is a wide-gap semiconductor unlike the narrow-gap IV-VI $Pb_{1-x}Ge_xTe$. The crystal structure is cubic zinc-blende-type. Cd(Zn) ion is surrounded by four Te ions tetrahedrally. The center of symmetry in this compound does not exist. When x=0.1, the crystal exhibits a dielectric anomaly at 393 K as shoen in Fig. 6. The peak value of dielectric constant (ε_{peak}) is only 50, which is smaller by about two orders than that of $BaTiO_3$ (~14000) and that of $Pb_{1-x}Ge_xTe$ (~1000). Because of the large E_g and the resistivity (~kΩ), a ferroelectric *D-E* hysteresis loop was successfully observed in the low-temperature phase. The direction of spontaneous polarization is along the apex of a tetrahedron, [111], which is reported as P_s= 0.0035 μC/cm² in their first paper, and 5 μC/cm² in the second paper. Because the ionic radius of Zn ion (0.83 Å) is smaller than that of Cd ion (1.03 Å), Zn ion also locates at the *off-center* position which deviates from the center of tetrahedra toward the apex. According to the result of EXAFS (X-ray absorption fine structure), it shifts by 0.04 Å [26]. It is considered that the ordering of *off-center ions* causes rhombohedral distortion of the cubic lattice by about 0.01 Å, and induces ferroelectricity.

In $Cd_{1-x}Zn_xTe$, the soft mode has not been observed and the dielectric anomaly is small. These dielectric properties are different from those found in $Pb_{1-x}Ge_xTe$, which are summarized in Table 1. These facts are consistent each other when one consider the LST (Lyddane-Sachs-Teller) relation ($\omega_{LO}^2/\omega_{TO}^2 = \varepsilon/\varepsilon_\infty$). In $Pb_{1-x}Ge_xTe$, the existence of soft mode is responsible for large dielectric anomaly. Although the behavior of *off-center ions* plays an important role in this ferroelectricity like $Pb_{1-x}Ge_xTe$, the occurrence of phase transition seems

to be driven in different way from that of $Pb_{1-x}Ge_xTe$, because of the different dielectric properties described above. Furthermore, the band gap is much larger than that of the narrow-gap ferroelectric semiconductors, which suggests that the electron-phonon coupling is not so strong in $Cd_{1-x}Zn_xTe$ solid solutions.

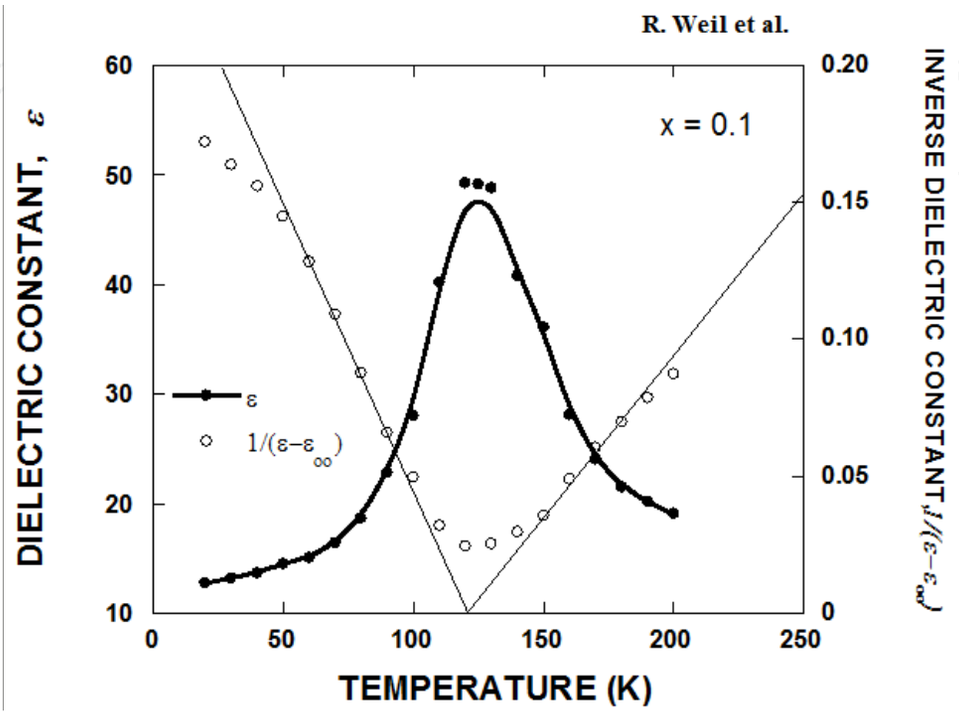

Figure 6. Temperature dependence of dielectric constant in $Cd_{1-x}Zn_xTe$ (x=0.1).

4.3. $Zn_{1-x}Li_xO$

Dielectric constants of $Zn_{1-x}Li_xO$ ceramics with x=0.09 show an anomaly at 470 K (T_c) (Fig. 7), although a high purity of ZnO does not show any anomaly from 20 K to 700 K [27]. The peak value of dielectric anomaly is 21 (x=0.1), which is the same order with $Cd_{1-x}Zn_xTe$ ($\varepsilon \sim 50$), but much smaller than ordinal ferroelectrics by 2~4 orders. This means that the dipole-dipole correlation accompanied with this ferroelectric phase transition is not so large in $Zn_{1-x}Li_xO$. In the measurement of *D-E* hysteresis loop, a small and clear hysteresis curve was observed. The spontaneous polarization varies by samples from 0.05 μC/cm² to 0.59 μC/cm². This is due to that the preferred orientation of the *c*-axis, the direction of P_s of the samples varies depending on samples. Naturally, powder of ZnO has egg-shaped grains which are elongated along the *c*-axis due to the anisotropy of elastic constants. Therefore, the orientation of the ceramic sample depends on the condition of the pressing process in the sample preparation. After the correction of the preferred orientation by using X-ray diffraction, the value of spontaneous polarizations of each sample converges to 0.9 μC/cm² as shown in Fig. 8 [28, 29]. The transition temperature, T_c, depends on the Li concentration. The phase diagram between T_c and x is shown in Fig. 9. As temperature increases, T_c becomes higher,which reminds us the phase diagram of quantum ferroelectrics such as $KTa_{1-x}Nb_xO_3$ and $Sr_{1-x}Ca_xTiO_3$.

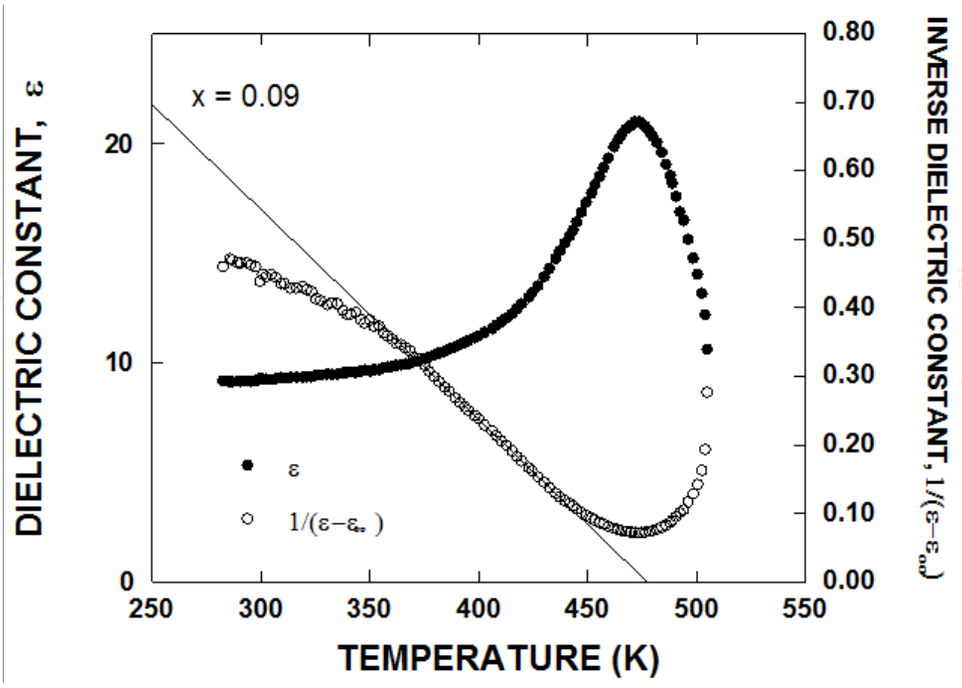

Figure 7. Temperature dependence of dielectric constant of $Zn_{1-x}Li_xO$ ceramics (x= 0.09).

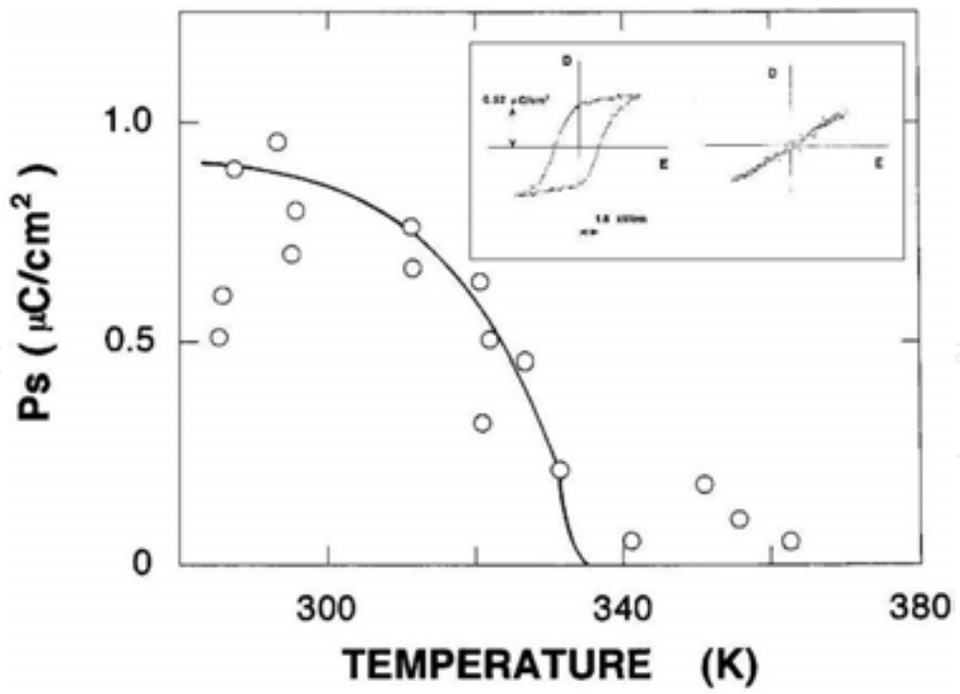

Figure 8. Temperature dependence of spontaneous polarization of $Zn_{1-x}Li_xO$ ceramics(x = 0.06). The inset is *D-E*hysteresis loop observed below (left) and above T_c (right).

http://dx.doi.org/10.5772/52304

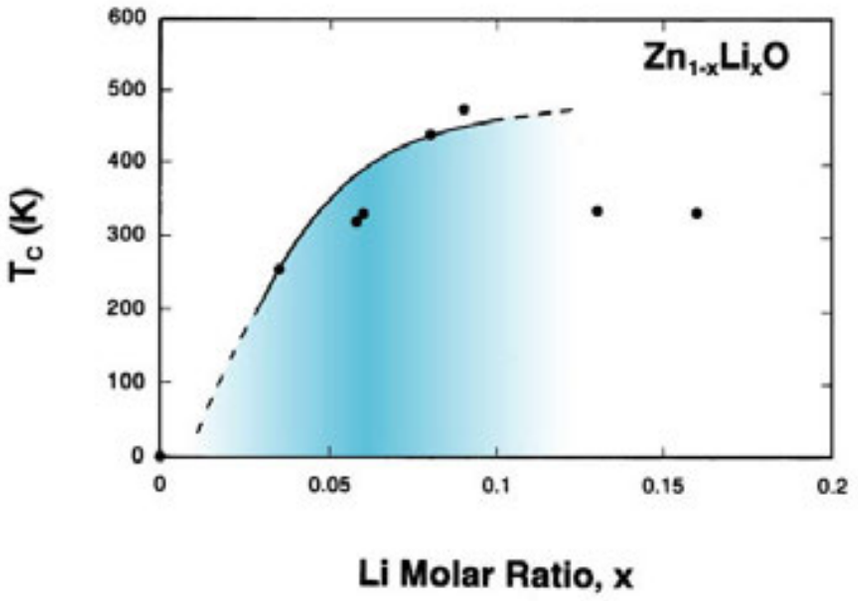

Figure 9. The T_c-x phase diagram of $Zn_{1-x}Li_xO$.

Specific heat anomaly is small at the ferroelectric-paraelectric phase transition temperature. The transition entropy ΔS is almost 0. If Li ions which substitute Zn ions occupy the off-center position and behave an order-disorder motion, ΔS must be about $R\ln 2$. If the nature of the transition is displacive type, $\Delta S \doteq 0$. The observed thermal behavior suggests displacive nature, but, however, no soft mode was observed in Raman scattering measurement [30]. The small dielectric anomaly and the absence of soft mode are consistent each other, when we consider the LST-relation. Relaxation mode corresponding to an order-disorder motion has not been found also by Raman scattering [31]. These peculiar dielectric properties of $Zn_{1-x}Li_xO$ is resemble to those of $Cd_{1-x}Zn_xTe$. These evidences suggests a new type of ferroelectric phase transition.

	$Pb_{1-x}Ge_xTe$	**$Cd_{1-x}Zn_xTe$**	**$Zn_{1-x}Li_xO$**
Crystal Structure of Paraelectric Phase	Rock-salt (NaCl) ((*Fm*3*m*))	Zinc-blende - ((*F*43*m*))	Wurtzite ((*P*6$_3$*mc*))
Ferroelectric Phase	Rhombohedral ((*R*3*m*))	Rhombohedral ((*R*3*m*))	Wurtzite ((*P*6$_3$*mc*))
T_c (K) (x=0.1)	200	390	470
E_g (eV)	0.3	1.53	3.2
ρ (Ωm)	10	10^3	10^{10}
P_s (μC/cm^2)	-	5	0.9
Soft mode	○	×	×
ε_{peak}	10^3	50	21

Table 1. Dielectric properties of binary ferroelectric semiconductors.

5. Electronic ferroelectricity in ZnO

It is considered that the replacement of host Zn atoms by substitutional Li atoms plays an primary role for the appearance of ferroelectricity in ZnO. The problem is the effect of Li-doping. Here we consider the following two models [32].

i. Structural size-mismatch model

Pure ZnO is polar along the *c*-axis and has dipole moments in crystals. Because of the size-mismatch between Zn ion (the ionic radius: 0.74 Å) and Li ion (the ionic radius: 0.60 Å), substituted Li ions displace from the Zn positions. These displacements may force to induce extra dipole moments locally. It is considered that these local dipoles couple with dipoles of the mother ZnO crystal and the structural ordering of local dipoles triggers to induce a ferroelectric phase transition.

ii. Electronic model

According to the first-principle study by Corso *et al* [10], the hybridization between Zn 3*d* electron and O 2*p* electron plays an important role in dielectric properties of ZnO. As the Li atom has no *d*-electrons, it is considered that the partial replacement of Zn ions by Li ions changes the nature of d the *d-p* hybridization. Therefore this doping is considered to induce local extra dipole moments. These extra local dipoles couple with parent dipoles and induce a new type of ferroelectricity.

To clarify which model is effective in the appearance of ferroelectricity in ZnO, the following structural and dielectric measurements were performed.

5.1. Rietveld analysis of structural changes in $Zn_{1-x}Li_xO$ ceramics

Structural changes associated with Li-substitution were studied by X-ray powder diffraction [33]. Ceramic samples of $Zn_{1-x}Li_xO$ prepared by using a SPS (spark plasma sintering) method were used in this experiment. The nominal value of x is 0.1 for the first sample. The T_c of the sample was 470 K which is determined by dielectric constant measurements. The systematic check of the absence of possible reflections (h-k=3n and l= odd for (hkl), n = integer) suggests that the space group of the ferroelectric phase still remains $P6_3mc$, which is same as pure ZnO. The obtained pattern was analyzed by the Rietveld method including the Li concentration, x, as a refinable parameter. All parameters refined are shown in Table 2. The lattice constants are a = 3.2487(1) and c = 5.2050(1) Å at 293 K. The actual Li concentration x is determined to be 0.09. The final discrepancy factors were R_{wp}=7.4%, R_p=5.4% and R_I=5.9%. The Zn-O bond lengths are 1.988_7 Å along the c-axis and 1.973_5Å in the basal plane, respectively. This means that the bond length along the c-axis shows a decrease by an amount of 0.003 Å by Li-substitution in Li-doped ZnO. This lattice distortion is the order of 10^{-3} Å only, while the displacement of Ti ions is the order of 0.1 Å in well-known ferroelectric $BaTiO_3$. In this phase transition, the crystal symmetry does not change associated with Li-substitution and structural change is considerably small compared with the structural phase transition in typical ferroelectrics.

http://dx.doi.org/10.5772/52304

Atom	*x*	*y*	*z*	*B*	Occupation
Zn	1/3	2/3	0.3821(3)	0.52	0.91
Li	1/3	2/3	03821(3)	0.31	0.09
O	1/3	2/3	0	0.40	1.0

Table 2. Positional (*x,y,z*) and isotropic thermal (*B*) parameters in $Zn_{1-x}Li_xO$ at 293K.

5.2. Effect of Be and Mg dopants on T_c

The effect of dopants on T_c was studied based on the two models mentioned above. If the ionic size-mismatch between the substituted and the host ions is important for ferroelectricity, the introduction of Be ions should be more effective than Li and Mg doping. The ionic radii of Li^+, Be^{2+} and Mg^{2+} ions are 0.60 Å, 0.3 Å and 0.65 Å, respectively. If the changes in electronic configuration are important, the Mg^{2+} ion ($1s^22s^22p^6$) should play a different role from the isoelectronic Li^+ and Be^{2+} ions ($1s^2$). Dielectric constant measurements were done on Mg- and Be-doped ZnO ceramics [32]. A dielectric anomaly of $Zn_{0.9}Be_{0.1}O$ was found at 496 K, which is very similar to those observed in $Zn_{1-x}Li_xO$. However, $Zn_{1-x}Mg_xO$ samples show a clear decrease of T_c. The dielectric anomaly in 30% Mg-doped ZnO found at 345 K is 150 K lower than the Li-doped one. The concentration dependence of T_c of Be- and Mg-doped ZnO is summarized in Fig. 10. The series of dielectric measurements show that the introduction of Mg^{2+} suppresses T_c, while isoelectronic Be^{2+} shows almost the same T_c.

It is considered that the appearance of ferroelectricity in ZnO is primarily due to electronic origin. The change in *d-p* hybridization caused by Li-substitution is responsible for this novel ferroelectricity and dielectric properties.

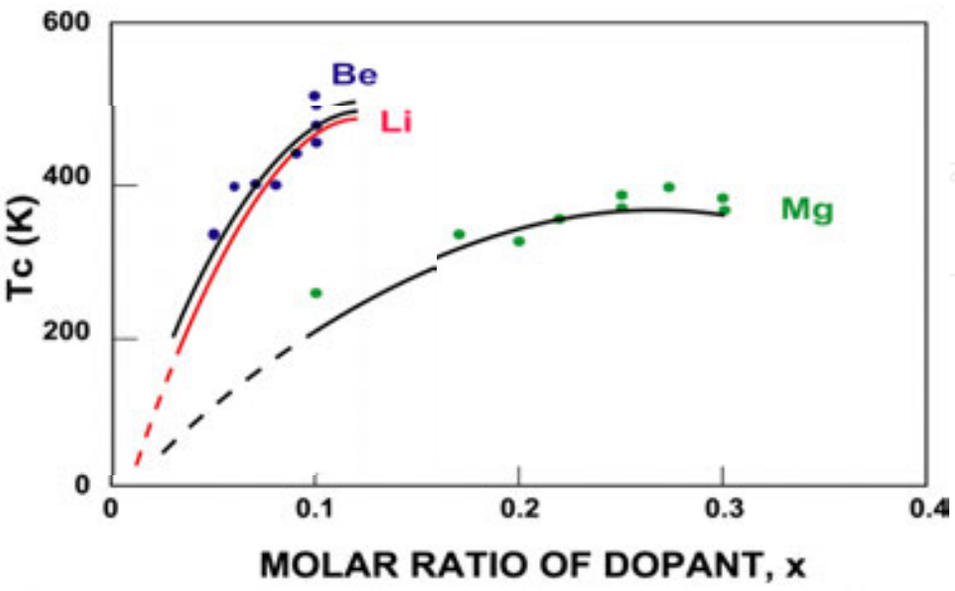

Figure 10. T_c*vs*. molar concentrations(*x*)of dopants, Li, Be and Mg in ZnO.

In the next section, we shall study the change in electronic distribution, especially in the nature of *d-p* hybridization by Li-doping directly by X-ray diffraction, and discuss new electronic ferroelectricity in ZnO.

6. X-ray study of electronic density distribution

X-ray diffraction measurements were performed for single crystals of pure ZnO and $Zn_{1-x}Li_xO$ at 297 K and 19 K in order to investigate the changes in the crystal structure and the electronic density distribution by Li-substitution in detail. Single crystal of pure ZnO was prepared by the hydrothermal method [34]. The content of excess Zn ions of obtained single crystal was 1.7 ppm and color was light yellowish (Fig. 11). In this hydrothermal method, it is rather difficult to add a large amount of Li ions into single crystal. In order to dope Li ions, several *c*-plate samples (0.16 mm thick) were annealed at an atmosphere of Li ions at 920 K for 24 hours. The light yellowish color of as-grown single crystal became transparent after this doping as shown in Fig. 12. Li concentration x was measured by chemical analysis and it is confirmed that $x = 0.082 \sim 0.086$.

Figure 11. Single crystal of as grown ZnO.

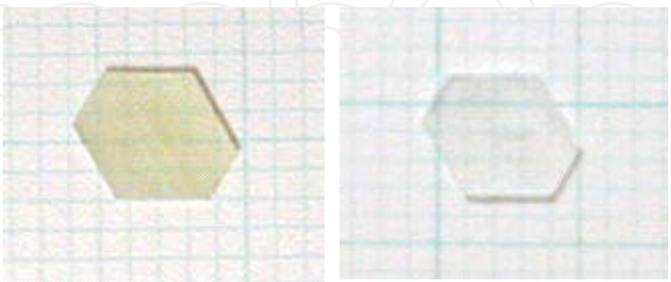

Figure 12. Single crystal of pure (left) and Li-doped ZnO (right).

Table 3 shows an experimental data of X-ray diffraction performed at room temperature (293 K) and low temperature (19 K) by using a He-gas closed-cycle cryostat (Cryogenic RC-110) mounted on a Huber off-center four-circle diffractometer to reduce the effect of

thermal vibration. The space group is confirmed to be $P6_3mc$ for both pure and Li-doped crystals. The Lorentz and polarization, thermal diffuse scattering (TDS) (the elastic constants used in TDS collection are C_{11}=20.96, C_{33}=21.09, C_{12}=12.10, C_{13}=10.51, C_{44}=4.243 [10^{11}dyn/cm^2], absorption (spherical) and extinction (anisotropic, type I) corrections were made. Crystal structures were refined using a full-matrix least squares program (RADIEL) [35].

	ZnO		$Zn_{1-x}Li_xO$	
Temperature	293 K	19 K	293 K	19 K
X-ray Radiation	AgKα	AgKα	MoKα	AgKα
$(\sin\theta/\lambda)_{max}$	1.36	1.36	1.00	1.27
Number of Reflections ($\|F_o\|$ "/> 3σ $\|F_o\|$)	3157	2533	1296	2377
μ*R*	1.91	2.84	7.67	3.96
R(*F*) (%)	2.61	3.84	3.05	3.62
$R_W(F)$ (%)	3.38	4.86	3.90	4.54
S	1.00	1.06	1.09	1.01

Table 3. Experimental data.

Accurate electron densities of single crystals of paraelectricZnO and ferroelectric Li-doped ZnO at 19 K were analyzed by the maximum-entropy method (MEM) [36]. The MEM analyses were performed using the MEED (maximum-entropy electron density) program [37].

6.1. Crystal structures of single crystals of ZnO and Li-doped ZnO at 293 K

The final positional parameters and thermal factors at 293 K are given with their estimated standard deviation in Table 4 [38]. The final discrepancy factors are *R*(*F*)=2.61 %, $R_w(F)$=3.38 % for ZnO, and *R*(*F*)=3.05 %, $R_w(F)$=3.90 % for $Zn_{1-x}Li_xO$. The lattice constants *a* and *c* of $Zn_{1-x}Li_xO$ become smaller than those of pure ZnO by 0.002 ~ 0.003 Å. Lattice distortion in $Zn_{1-x}Li_xO$ is only the order of 10^{-3} Å along the polar axis, which is consistent with that of ceramic sample measured by thermal expansion [39]. These changes are regarded as the changes associated with ferroelectric phase transition because Li-doped ZnO is ferroelectric phase and pure ZnO is paraelectric phase. In $BaTiO_3$, the lattice constants change by 0.02 Å. In ZnO, changes in the lattice constants are smaller than that of $BaTiO_3$ by one order. The thermal factors U_{33} of Zn and O atoms in $Zn_{1-x}Li_xO$ are smaller than U_{11} by 25-35 %, although those values in pure ZnO are almost same. This implies that the thermal vibration in $Zn_{1-x}Li_xO$ is suppressed along the *c*-axis. But in ZnO, the effect from bonding electron is also included in the thermal factors since strong covalence exists. The effects of thermal vibration and bonding electron cannot be distinguished at 297 K. The Li concentration *x*, the positional parameter *u* and isotropic thermal factor *U* of Li are refined after all the other parameters are determined. Two cases are assumed for the Li position: the first is the interstitial position

and the second is host Zn position. The discrepancy factor became larger when Li locates at interstitial Li position than Zn position. Therefore, present results support that Li substitutes Zn. The precise refinement shows that Li locates at the off-center position from the Zn position by 0.02 Å in $Zn_{1-x}Li_xO$ along the *c*-axis.

ZnO (a=3.2489(1) Å, c=5.2049(3) Å) at 293 K							
	x	*y*	*z*	U_{11}	U_{33}	U_{eq}	Occupation
Zn	1/3	2/3	0.3815(1)	0.0086(1)	0.0088(1)	0.0087(1)	1.0
O	1/3	2/3	0	0.0085(1)	0.0088(1)	0.0086(1)	1.0
$Zn_{1-x}Li_xO$ (a=3.2467(3) Å, c=5.2032(1) Å) at 293 K							
	x	*y*	*z*	U_{11}	U_{33}	U_{eq}	Occupation
Zn	1/3	2/3	0.3804(3)	0.0075(1)	0.0055(1)	0.0068(1)	0.914
Li	1/3	2/3	0.376(36)			0.0036(48)	0.086
O	1/3	2/3	0	0.0088(3)	0.0057(41)	0.0078(3)	0.957

Table 4. Crystal structure of ZnO and $Zn_{1-x}Li_xO$ at 293 K.(The form of thermal factors are $\exp[-2\pi^2(U_{11}a^{*2}h^2 + U_{22}b^{*2}k^2 + U_{33}c^{*2}l^2 + 2U_{12}a^*b^*hk + 2U_{23}b^*c^*kl + 2U_{31}c^*a^*lh)]$ for anisotropic (Zn and O) and $\exp(-8\pi^2U_{eq}\sin^2\theta/\lambda)$ for isotropic (Li) atoms.)

The bond lengths and angles of ZnO_4 group are shown in Table 5. The Zn-O bond length does not change in the basal plane, but becomes short along the *c*-axis by an amount of 0.007 Å by Li-substitution.

	Bond length		**Bond Angle**	
	Apical	Basal	Apical	Basal
ZnO	1.986(1) Å	1.975(1) Å	108.20(3)°	110.71(3)°
$Zn_{1-x}Li_xO$	1.979(1) Å	1.975(1) Å	108.37(4)°	110.55(4)°

Table 5. Bond lengths and angles in ZnO and $Zn_{1-x}Li_xO$ at 293 K.

The distributions of electronic density around Zn and O atoms at 293 K are obtained by using Fourier analysis (Fig. 13). The difference Fourier maps between observed distribution ϱ_{obs} and calculated distribution ϱ_{cal} in the (110) plane are shown in Fig. 14. Since the bonding electron is not distributed spherically in ZnO, the section of the bonding electron appears in the difference map. It is seen that there are large negative distributions (blue region) around Zn atom along the *c*-axis in $Zn_{1-x}Li_xO$. This suggests that the core electrons disappear from the Zn atom. The broadening of map due to anharmonic thermal vibrations is also appreciated. The positive electronic density is observed near the O atom. It corresponds to the antibonding orbital of O 2*p*-electron.

http://dx.doi.org/10.5772/52304

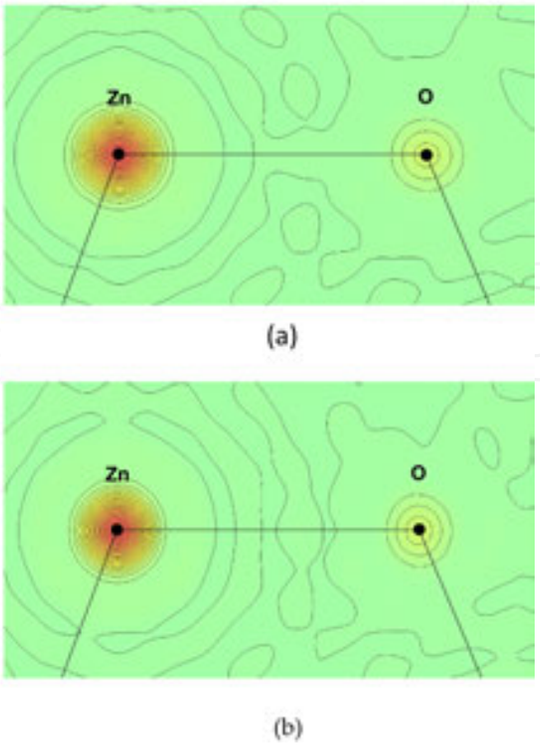

Figure 13. The charge density maps of (a) ZnO and (b) $Zn_{1-x}Li_xO$ at 293 K in the (110) plane obtained by Fourier analysis.

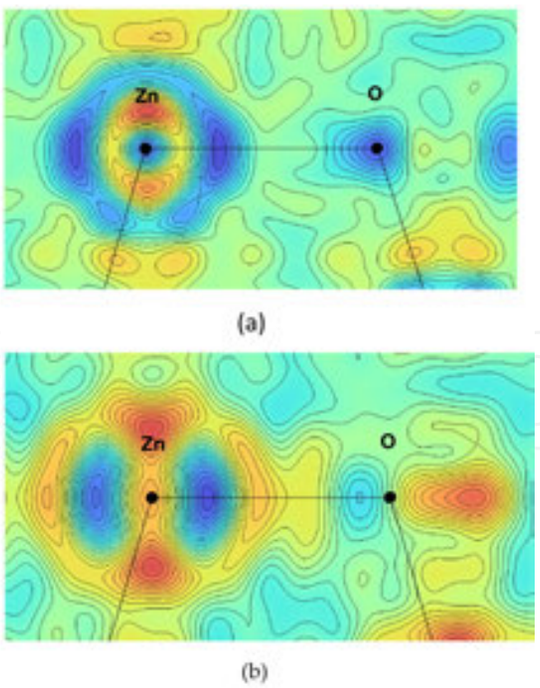

Figure 14. The difference fourier maps of charge densities of (a) ZnO and (b) $Zn_{1-x}Li_xO$ at 293 K in the (110) plane with a contour increment of 0.2 *e*/ Å ^{3}. Bluish cold color means negative charge density and reddish warm region is positive charge density.

6.2. Crystal structures at 19 K

Crystal structures at low temperature are shown in Table 6 [38]. The final discrepancy factors are $R(F)$=3.84 %, $R_w(F)$=4.86 % for ZnO, and $R(F)$=3.62 %, $R_w(F)$=4.54 % for $Zn_{1-x}Li_xO$. Li ion shifts from the Zn position by 0.08 Å at 19 K, which is four times larger than that at r. t.. The Zn-O bond lengths decrease by an amount of 0.002 Å along both basal and apical axes in $Zn_{1-x}Li_xO$, while their bond angles are almost the same in both crystals (Table 7 and Fig. 15). The Fourier and difference maps of electronic distribution are shown in Figs. 16 and 17. Comparing with the result of 293 K, bonding electrons are clearly observed around the center of Zn-O bond in both crystals. In $Zn_{1-x}Li_xO$, negative distribution is observed around Zn atom, whose shape corresponds to Zn-3d_z^2-orbital. It suggests the disappearance of 3*d*-electrons from Zn atom in $Zn_{1-x}Li_xO$. The positive density near O atoms corresponds to the 2*p*-orbital of O atom.

ZnO (a=3.2465(8) Å, c=5.2030(19) Å) at 19 K							
	x	*y*	*z*	U_{11}	U_{33}	Occupation	
Zn	1/3	2/3	0.3812(1)	0.0033(1)	0.0032(1)	1.0	
O	1/3	2/3	0	0.0041(1)	0.0048(2)	1.0	
$Zn_{1-x}Li_xO$ (a=3.2436(5) Å, c=5.1983(30) Å) at 19 K							
	x	*y*	*z*	U_{11}	U_{33}	U_{eq}	Occupation
Zn	1/3	2/3	0.3811(2)	0.0032(1)	0.0026(1)	0.0030(1)	0.914
Li	1/3	2/3	0.366(12)	-	-	0.0036(48)	0.086
O	1/3	2/3	0	0.0053(3)	0.0043(3)	0.0050(2)	0.957

Table 6. Crystal structure of ZnO and $Zn_{1-x}Li_xO$ at 19 K.(The form of thermal factors are $\exp[-2\pi^2(U_{11}a^{*2}h^2 + U_{22}b^{*2}k^2 + U_{33}c^{*2}l^2 + 2U_{12}a^*b^*hk + 2U_{23}b^*c^*kl + 2U_{31}c^*a^*lh)]$ for anisotropic (Zn and O) and $\exp(-8\pi^2U_{eq}\sin^2\theta/\lambda)$ for isotropic (Li) atoms.)

	0.957		**0.957**	
	Apical	Basal	Apical	Basal
ZnO	1.983(2) Å	1.974(1) Å	108.25(4)°	110.66(4)°
$Zn_{1-x}Li_xO$	1.981(2) Å	1.972(1) Å	108.27(3)°	110.65(3)°

Table 7. Bond lengths and angles in ZnO and $Zn_{1-x}Li_xO$ at 19 K.

http://dx.doi.org/10.5772/52304

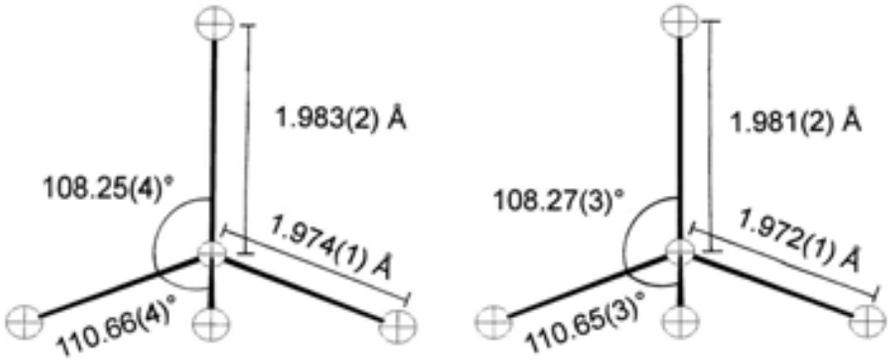

(a) Pure ZnO (b) Li-doped ZnO

Figure 15. Structural Changes of ZnO_4 group at 19 K. The shift of Li ion is 0.08 Å from the Zn position.

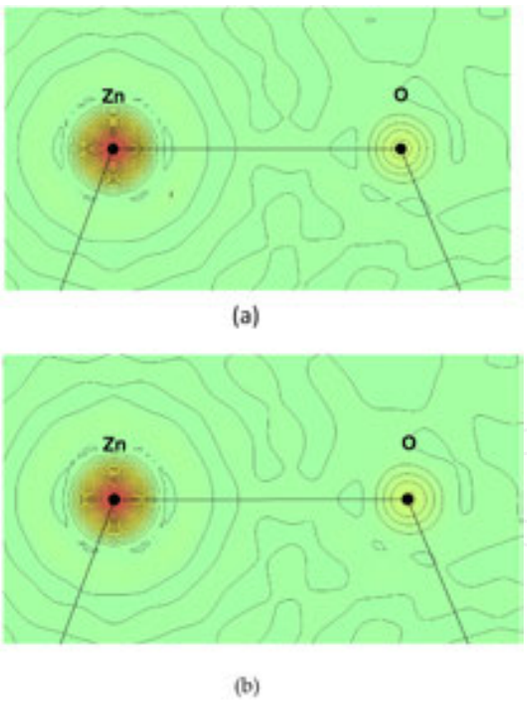

Figure 16. The charge density maps of (a) ZnO and (b) $Zn_{1-x}Li_xO$ at 19 K in the (110) plane obtained by Fourier analysis.

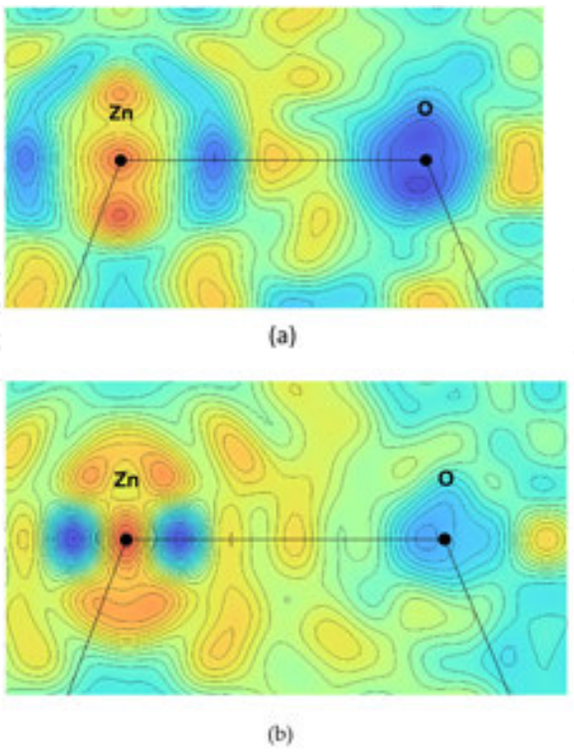

Figure 17. The difference maps of charge densities of (a) ZnO and (b) $Zn_{1-x}Li_xO$ at 19 K in the (110) plane with a contour increment of 0.2 *e*/ Å ^{3}. Bluish cold color means negative charge density and reddish warm color region is positive charge density.

6.3. Bond electron densities at 19 K

The discrepancy factors of MEM analysis for pure ZnO at 19 K are $R(F)$=1.20 % and $R_w(F)$=1.39 % [40]. The electron density map of ZnO in the (110) plane is shown in Fig. 18(b). The covalent character of Zn-O bonds is clearly observed. Charge densities at the center of Zn-O bonds are 0.58 *e*/ Å ^{3} for the apical bond, and 0.56 *e*/Å ^{3} for the basal one. The density of bonding electron of the apical bond is larger than that of the basal by 3.6 %. The electron density of O atom distorts toward the Zn atom along the *c*-axis. The electron density of Zn atom elongates to the third nearest O atom.

The final discrepancy factors for the ferroelectric $Zn_{1-x}Li_xO$ at 19 K are $R(F)$=0.87 % and $R_w(F)$=0.85%. The electron density map of $Zn_{1-x}Li_xO$ in the (110) plane is shown in Fig. 18(c). The covalent character of Zn-O bonds is also seen in $Zn_{1-x}Li_xO$. Charge densities of the Zn-O at the saddlepoint are 0.46 *e*/ Å ^{3} for the apical bond, and 0.49 *e*/ Å ^{3} for the basal one. Each value is smaller than that of pure ZnO. It is considered that this may be due to the decrease of total charge by Li-substitution. The density of bonding electron of the basal bond is larger than that of the apical by 6.5 %, on the contrary to the case of ZnO. The electron density of O atom is distorted anisotropically, similar to the pure ZnO, but the direction is opposite. The extension of Zn atom toward the third nearest O atom, which is observed in ZnO, was not detected in $Zn_{1-x}Li_xO$.

http://dx.doi.org/10.5772/52304

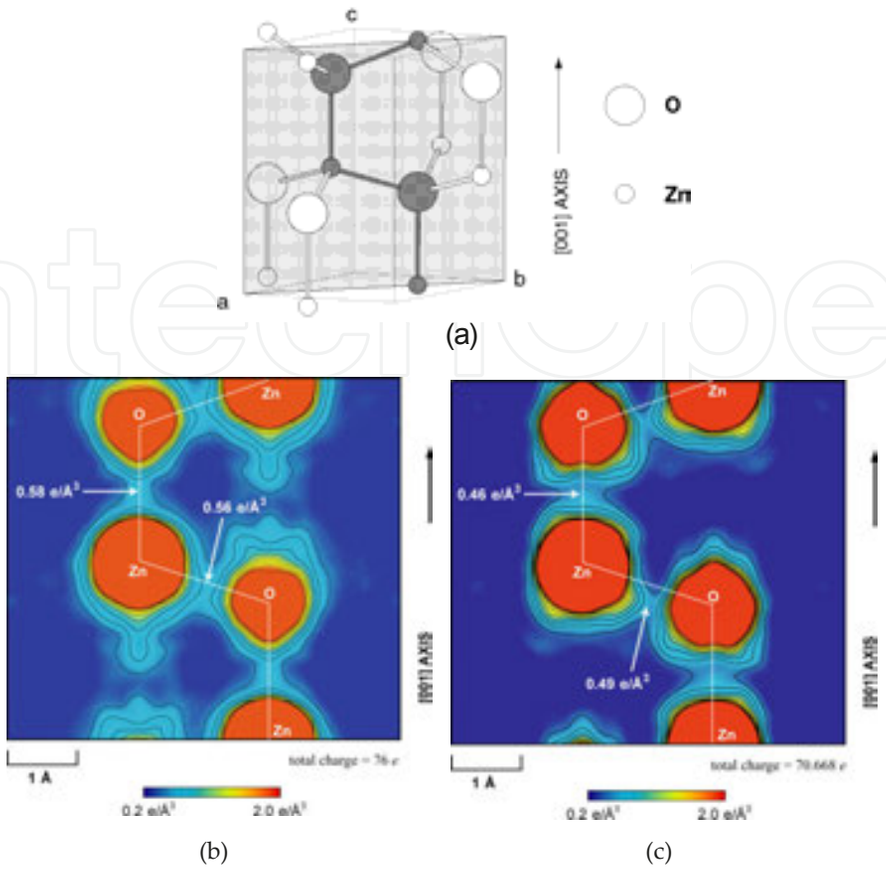

Figure 18. The electronic Distribution by MEM method. (a) The (110) plane of ZnO. Shaded atoms are included in the plane.(b)The MEM charge density map of ZnO at 19 K in the (110) plane. (c) The MEM charge density map of $Zn_{0.914}Li_{0.086}O$ at 19 K in the (110) plane. Contours are drawn from 0.4 *e*/ Å^3 at 0.2 e/ Å^3 intervals.

6.4. Difference between Li-doped ZnO and pure ZnO

The difference of the charge densities between two crystals is calculated by subtracting the MEM charge densities of pure ZnO from those of $Zn_{1-x}Li_xO$ as in Fig. 19 [40]. The values of MEM charge densities of pure ZnO are normalized by multiplying 0.930, because the total charges of two crystals are different. The positive and negative peaks were observed around the O atom. This is due to the shift of O atom from the host position opposite to the Zn atom along the *c*-axis in $Zn_{1-x}Li_xO$. Four negative peaks are observed around the Zn atom. These peaks correspond to the Zn 3*d*-orbitals and suggest that the 3*d*-electrons disappear from the Zn site, compared with wave functions of Zn 3*d*- and O 2*p*-orbitals of ZnO obtained by DV-Xα calculation in Fig. 20. This result is the same as that calculated by the Fourier synthesis previously. The bonding region around the apical and the basal Zn-O bonds is covered by positive electron distribution. This implies that the Zn 3*d*-electrons transfer to the bonding electrons in $Zn_{1-x}Li_xO$.

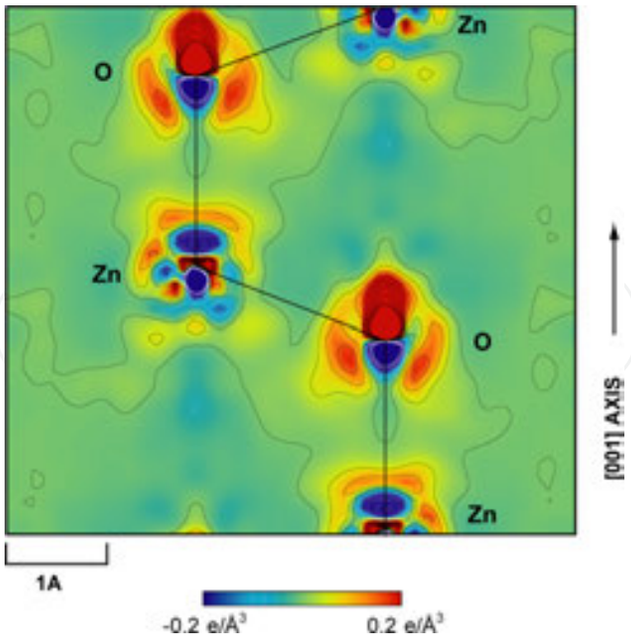

Figure 19. The difference map between MEM charge densities of $Zn_{1-x}Li_xO$ and ZnO at 19 K in the (110) plane. Contours are drawn from -5.0 *e*/ Å^3 to 5.0 *e*/ Å^3 at 0.5 *e*/ Å^3 intervals. Shaded area eith reddish color indicates positive charge.

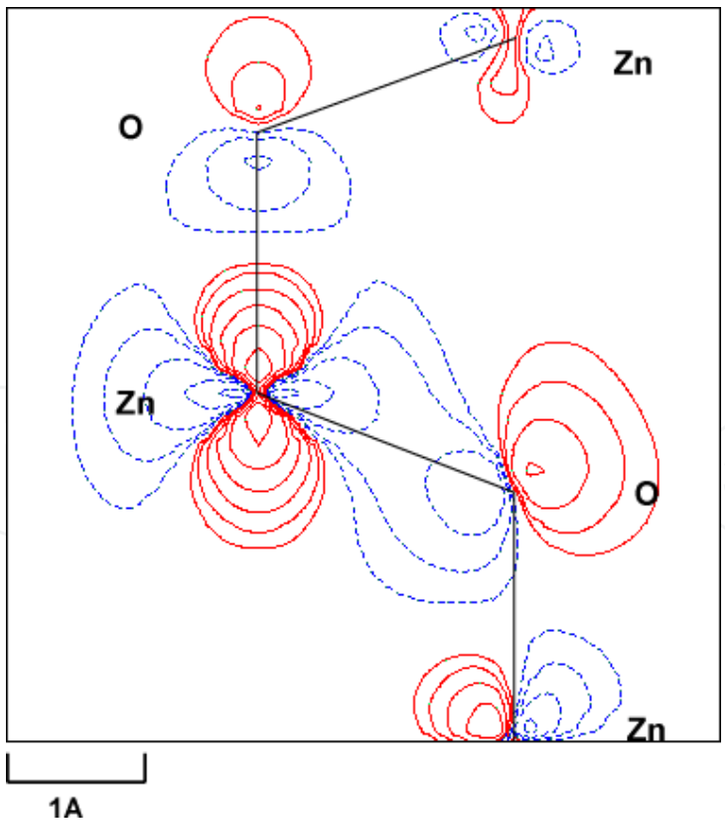

Figure 20. Wave functions of Zn 3*d*- and O 2*p*-orbitals of ZnO obtained by DV-Xα calculation. Red lines indicate the positive and Blue lines indicate the negative area.

In Li-doped ZnO, negative peaks around Zn atom corresponding to $3d_z^2$ orbital were observed in difference Fourier map, and also in the MEM difference map between the ferroelectric phase and the paraelectric phase. These results may be related to the existence of localized *d*-holes in Li-doped ZnO. It is considered that $3d_z^2$ electrons transfer to bonding region and play a role for contribution for the covalence observed from the result of the MEM analysis. Furthermore, the antibonding orbital of 2*p* electron is observed in difference Fourier map of Li-doped ZnO. It is suggested that the interaction between *d*-holes and *p*-electrons should be closely related to the appearance of the ferroelectricity in Li-doped ZnO.

7. Discussion

The ferroelectric phase transition accompanies with structural distortions in usual ferroelectrics. Portengen, Ostreich and Sham reported the theory of electronic ferroelectricity [41], which examined possibilities of electronic ferroelectricity, based on the spinless Falikov-Kimball (FK) model [42] with a *k*-dependence hybridization in Hartree-Fock approximation. The FK model introduces two types of electrons, itinerant *d*-electrons and localized *f*-electrons. The valence transition is driven by on-site Coulomb repulsion between the *d*-electrons and *f*-electrons. They found that the Coulomb interaction between itinerant *d*-electrons and the localized *f*-electrons give rise to an excitonic$<d^{+}f>$ expectation value, which breaks the center of symmetry of the crystal and leads to electronic ferroelectricity in mixed-valent compounds. In this electronic model, the transition involves a change in the electronic structure rather than the structural one. The estimated spontaneous polarization is of the order of 10 $\mu C/cm^2$, which is comparable to those in displacive type ferroelectrics such as $BaTiO_3$.

In the case of Li-doped ZnO, the *d-p* hybridization should be changed by Li-doping. The *d*-holes and itinerant electrons should be closely related to the appearance of Li-doped ZnO. It should be further detailed studies would be necessary whether this proposed theory is applicable for the electronic ferroelectricity found in ZnO or not.

Recently Glinchuk *et al* propose the mechanism of impurities induced ferroelectricity in nonperovskite semiconductor matrices due to indirect dipole interaction via free carriers [43]. They showed that the ferroelectricity in Li-doped ZnO might appear due to indirect interaction of dipoles, formed by off-center impurities, *via* free charge carriers, namely, the Ruderman–Kittel–Kasuya–Yosida (RKKY)-like indirect interaction of impurity dipoles *via* free charge carriers. They estimated that the typical semiconducting concentration of the carriers like 10^{17} cm^{-3} is sufficient for the realization of the ferroelectricity. The finite conductivity does not mean complete destruction of possible ferroelectric order and shows rather many interesting effects. In this theory, they have succeeded to obtain the spontaneous polarization and the phase diagram of T_c*vs*. impurity molar ratio (*x*) as shown in Fig. 21.

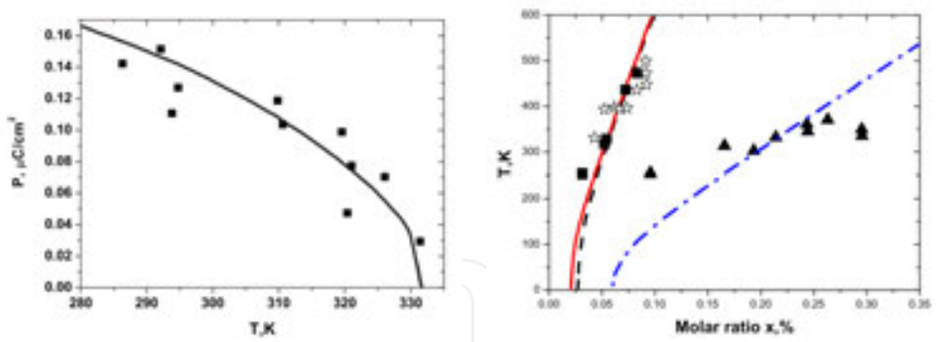

Figure 21. The calculated spontaneous polarization and the phase diagram of T_c*vs.* impurity molar ratio (x) after Glinchuk et al [36].

Experimental results suggest the existence of localized *d*-holes and *p*-electrons in Li-doped ZnO. We consider that the interaction between *d*-holes and *p*-electrons may be related to the appearance of the ferroelectricity in Li-doped ZnO. However, there are many proposals for this peculir novel ferroelectricity in ZnO. Scott and Zubko have pointed out the possibility of a classic electret mechanism for Li-doped ZnO[44]. Tagantsev discussed a Landau theory, where a crystal on cooling from a state with polar symmetry exhibits a maximum of dielectric permittivity and *D-E* hysteresis loops [45]. He proposed that these ferroelectric like phenomena corresponds to the case for Li-doped ZnO. Furthermore, the multiferroic behavior has been reported in impurity-doped ZnO [46]. At present, further detailed experiments should be expected to clarify the nature of Li-doped ZnO.

8. Conclusion

Dielectric properties and crystal structures and electron density distributions studied on pure ZnO and $Zn_{1-x}Li_xO$ by the precise X-ray diffraction are reviewed in comparison with ferroelectric semiconductors $Pb_{1-x}Ge_xTe$ and $Cd_{1-x}Zn_xTe$. It is considered that the appearance of ferroelectricity in ZnO is primarily due to electronic origin. The change in *d-p* hybridization caused by Li-substitution is considered to be responsible for this novel ferroelectricity and dielectric properties. Although the ferroelectric phase transition accompanies with structural distortions in usual ferroelectrics, the structural changes observed in $Zn_{1-x}Li_xO$ are the order of 10^{-3} Å. The clear change of Zn 3*d*-electron is observed. It suggests Zn 3*d*-electron of $Zn_{1-x}Li_xO$ transfers from Zn atom to the bonding. The positive electronic density is observed near the O atom. It corresponds to the antibonding orbital of O 2*p*-electron. These results suggest the existence of localized *d*-holes and *p*-electrons in Li-doped ZnO. It may be probable that the interaction between *d*-holes and *p*-electrons may be related to the appearance of the ferroelectricity in Li-doped ZnO.

For long time, the importance of electronic contribution has been pointed out in the field of ferroelectrics, since the simple superposition of electronic polarizability does not hold in many ferroelectric substances. Many efforts have been done in vain because of complexity of

crystal structures of ferroelectrics. As the crystal structure of ZnO is very simple, the electronic contribution could be observed rather easily. It is considered that this result is the first example to discuss the electronic contribution for ferroelectricity.

Author details

Akira Onodera and Masaki Takesada

Department of Physics, Faculty of Science, Hokkaido University, Sapporo, Japan

References

[1] Klingshirn C F, Meyer B K, Waag A, Hoffmann A and Geurts J. Zinc Oxide From Fundamental Properties Towards Novel Applications. Springer, 2010.

[2] Yao T (ed.). ZnO Its Most Up-to-date Technology and Application, Perspectives (in japanese). CMC Books, 2007.

[3] Heiland G. Mollwo E and Stockmann F. Solid State Phys 1959; 81: 193.

[4] Campbell C. Surface Acoustic Wave Devices and Their Signal Processing Application. San Diego: Academic Press; 1989.

[5] Hirshwald W. Current Topics Mater Sci 1981; 7, 143.

[6] Tsukazaki A, Ohtomo A, Onuma T, Ohtani M, Makino T, Sumiya M, Ohtani K, Chichibu S F, Fuke S, Segawa Y, Ohno H, Koinuma H and Kawasaki M. Nature Materials 2005; 4: 42.

[7] Joseph M, Tabata H and Kawai T. Jpn J Appl Phys 1999; 38: L1205.

[8] Bilz H, Bussmann-Holder A, Jantsch W and Vogel P. Dynamical Properties of IV-VI

[9] Compounds. Berlin: Springer-Verlag; 1983.

[10] Weil R, Nkum R, Muranevich E and Benguigui L. Phys Rev Lett 1989; 62: 2744.

[11] Onodera A, Tamaki N, Kawamura Y, Sawada T and Yamashita H. Jpn. J Appl Phys 1996; 35: 5160.

[12] Abrahams C S and Bernstein L J. Acta Cryst 1969; B25: 1233.

[13] Corso D A, Posternak M, Resta R and Baldereshi A. Phys Rev 1994; B50: 10715.

[14] Zakharov O, Rudio A, Blase X, Cohen L M and Louie G S. Phys Rev1994; B50: 10780.

[15] Massida S, Resta R, Posternak M and Baldereschi A. Phys Rev 1995; B50.

[16] Osikiri M and Aryasetiawan F. J Phys Soc Jpn 2000; 69: 2123.

[17] Minami T, Nanto H and Tanaka S. Jpn J Appl Phys 1984; 23: L280.

[18] Laudise A R, Kolb D E and Caporaso J A. J Am Ceram Soc 1964; 47: 9.

[19] Kolb D E and Laudise A R. J Am Ceram Soc 1966; 49: 302.

[20] Yang CK and Dy S K. Solid State Commun 1993; 88: 491.

[21] Usuda M, Hamada N, Kotani T and Schilfgaarde M. Phys Rev 2001; B66: 075205.

[22] Zhang B S, Wei S -H and Zunger A. Phys Rev 2001; B63: 075205.

[23] Tamaki N, Onodera A, Sawada T and Yamashita H. J Kor Phys 1966; 29: 668.

[24] Onodera A, Tamaki N, Jin K and Yamashita H. Jpn J Appl Phys 1997; 36: 6008.

[25] Islam T Q and Bunker A B. Phys Rev Lett 1987; 59: 2701.

[26] Benguigui L, Weil R, Muranevich E, Chack A and Fredj E. J Appl Phys 1993; 74:513.

[27] Terauchi H, Yoneda Y, Kasatani H, Sakaue K, Koshiba T, Murakami S, Kuroiwa Y, Noda Y, Sugai S, Nakashima S and Maeda H. Jpn J Appl Phys 1993; 32: 728.

[28] Onodera A, Yoshio K, Satoh H, Yamashita H and Sakagami N. Jpn. J. Phys. Phys. 1998; 37; 5315.

[29] Onodera A, Tamaki N, Satoh H, Yamashita H and Sakai A. Ceramic Transactions 1999; 100; 77.

[30] Onodera A and Satoh H. Frontiers in Science and Technology – Ferroelectrics Vol. 1, Stefan University Press, 2002; 93.

[31] Islam E, Sakai A and Onodera A. J Phys Soc Jpn 2001; 70: 576.

[32] Kagami D, Takesada M, Onodera A and Satoh H. J Kor Phys 2011; 59: 2532.

[33] Hagino S, Yoshio K, Yamazaki T, Satoh H, Matsuki K and Onodera A. Ferroelectrics 2001; 264: 235.

[34] Onodera A, Yoshio K, Satoh H, Tamaki T, Takama T, Fujita M and Yamashita H. Ferroelectrics 1999; 230: 465.

[35] Sakagami N. J Cryst Growth 1990; 99: 905.

[36] Coppens P, Guru Row N T, Leung P, Stevens D E, Becker J P and Yang W Y. Acta Crystallogr 1979; A35: 63.

[37] Sakata M and Sato M. Acta Crystallogr 1990; A46: 263.

[38] Kumazawa S, Kubota Y, Tanaka M, Sakata M and Ishibashi Y. J Appl Cryst 1993; 26: 453.

[39] Yoshio K, Onodera A, Satoh H, Sakagami N and Yamashita H. Ferroelectrics 2001; 264; 133.

[40] Onodera A, Tamaki N, Satoh H and Yamashita H. Ferroelectrics 1998; 217: 9.

[41] Yoshio K, Onodera A, Satoh H, Sakagami N and Yamashita H. Ferroelectrics 2002; 270; 357.

[42] Portengen T, Ostreich Th and Sham J L. Phys Rev 1996; B54: 17452.

[43] Falicov M L and Kimball C J. Phys Rev Lett 1969; 22: 997.

[44] Glinchuk D M, Kirichenko V E, Stephanovich A V and Zaulychny Y B. Appl Phys 2009; 105: 104101.

[45] Scott F J and Zubko P. IEEE Xplore 2005; ISE-12 (12th International Symposium on Electrets): 113-116.

[46] Tagantsev K A. Appl Phys Let 2008; 93: 202905.

[47] Yang C Y, Zhong F C, Wang H X, He B, Wei Q S, Zeng F and Pan F. Appl Phys 2008; 104: 064102.

IntechOpen